



Shaped pulses for transient compensation in quantum-limited electron spin resonance spectroscopy



Sebastian Probst^a, Vishal Ranjan^a, Quentin Ansel^b, Reinier Heeres^a, Bartolo Albanese^a, Emanuele Albertinale^a, Denis Vion^a, Daniel Esteve^a, Steffen J. Glaser^{c,d}, Dominique Sugny^b, Patrice Bertet^{a,*}

^aQuantronics Group, SPECT, CEA, CNRS, Université Paris-Saclay, CEA Saclay 91191, Gif-sur-Yvette Cedex, France

^bUniversité de Bourgogne Franche-Comté, Laboratoire Interdisciplinaire Carnot de Bourgogne, CNRS UMR 6303, 21078 Dijon Cedex, France

^cDepartment of Chemistry, Technische Universität München, Lichtenbergstraße 4, D-85747 Garching, Germany

^dMunich Center for Quantum Science and Technology (MCQST), Schellingstr. 4, D-80799 München, Germany

ARTICLE INFO

Article history:

Received 1 March 2019

Revised 8 April 2019

Accepted 9 April 2019

Available online 11 April 2019

Keywords:

Electron paramagnetic resonance

Arbitrary waveform generator

Shaped pulses

Superconducting resonators

Quantum limited amplifier

ABSTRACT

In high sensitivity inductive electron spin resonance spectroscopy, superconducting microwave resonators with large quality factors are employed. While they enhance the sensitivity, they also distort considerably the shape of the applied rectangular microwave control pulses, which limits the degree of control over the spin ensemble. Here, we employ shaped microwave pulses compensating the signal distortion to drive the spins faster than the resonator bandwidth. This translates into a shorter echo, with enhanced signal-to-noise ratio. The shaped pulses are also useful to minimize the dead-time of our spectrometer, which allows to reduce the wait time between successive drive pulses.

© 2019 The Authors. Published by Elsevier Inc. This is an open access article under the CC BY license (<http://creativecommons.org/licenses/by/4.0/>).

1. Introduction

Electron spin resonance (ESR) spectroscopy allows to analyze the composition and structure of paramagnetic samples [1]. In the inductive detection method, the sample is coupled to a resonant microwave cavity of frequency ω_0 . When the spins are tuned to ω_0 by application of a magnetic field B_0 , they interact with the magnetic component of the intra-cavity microwave field $B_1(t)$. After being driven by appropriate microwave pulse sequences, their Larmor precession dynamics induces the subsequent emission of weak microwave spin-echo signals, which carry information on the properties of the paramagnetic species present in the sample.

The cavity has several roles in this process. It amplifies the B_1 driving field by a factor proportional to \sqrt{Q} (Q being the resonator quality factor), which lowers the incident microwave power requirements. It also amplifies the emitted spin-echo signals by the same factor, which conversely enhances detection sensitivity. On the other hand, the cavity bandwidth $\kappa = \omega_0/Q$ limits both the spin excitation and spin detection bandwidths, which can be

a severe issue since typical electron spin linewidths may exceed κ by far. The cavity also causes transients in the drive fields which limit the degree of control achieved on spin dynamics, and whose characteristic time scale is given by the cavity field amplitude damping time $2/\kappa$. As a result, the cavity quality factor needs to be carefully optimized for the purpose of a given experiment.

A number of these issues can be mitigated by the use of drive pulses with a more complex time-dependence than a simple rectangular pulse (so-called shaped pulses) [2,3], as schematically shown in Fig. 1. Thanks to modern arbitrary waveform generators (AWG) [4], microwave pulses with arbitrary time-dependent amplitude and phase can be generated. If the transfer function between the AWG and the intra-cavity field is known, it is possible to compute the drive pulse shape needed to obtain arbitrary intra-cavity field temporal profiles. This strategy in principle eliminates all the drive pulse distortions caused by the cavity; in particular, spins can be driven with a bandwidth much larger than κ using shaped pulses [5]. Cavity filtering of the signal emitted by the spins, however, remains unavoidable [5].

The use of shaped pulses [6] has been proposed and demonstrated first in nuclear magnetic resonance spectroscopy [2,3,7–9]. They have then been applied in ESR spectroscopy [10] for cavity ringdown suppression [11,4,12], wide-band Fourier-transform

* Corresponding author.

E-mail address: patrice.bertet@cea.fr (P. Bertet).

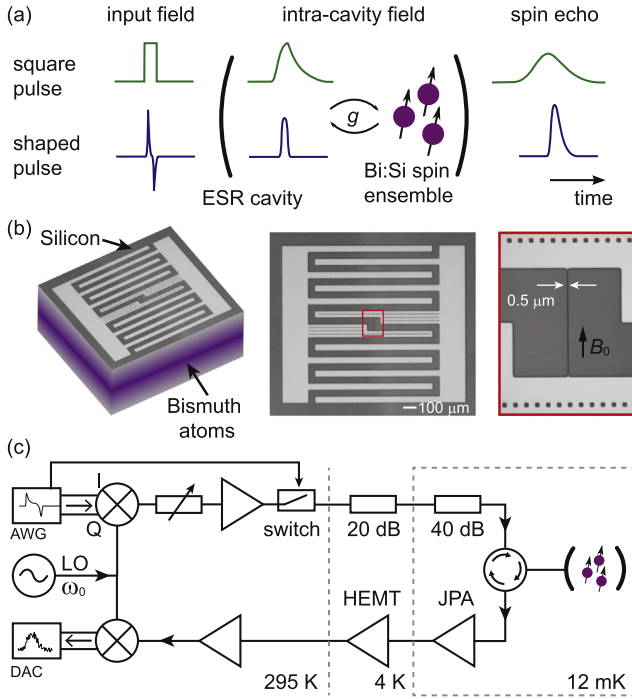


Fig. 1. (a) Basic concept. A short microwave pulse with a rectangular envelope (left green line) is sent onto an ESR cavity and is subsequently distorted by the cavity's transfer function. The resulting intracavity field (center green line) then drives the spins for much longer than intended resulting in spin-echo signals which are stretched in time (right green line). In contrast, if a tailored shaped pulse is employed (left blue line), the cavity distortion is compensated. A short intracavity field (center blue line) now drives the spins resulting in wide-band spin manipulation and shorter echo duration. (b) Schematics and optical images of the LC resonator used in the experiment. Dark areas represent the Si substrate while light areas are made of Al. Bi spins are implanted everywhere below the Si surface, in a box-like profile at a depth ~ 100 nm. The resonator active area is a 0.2 pL volume around the 100 μm -long, 500 nm-wide inductance. (c) Technical implementation. Shaped drive pulses are generated by modulating the output of a continuous-wave microwave generator (LO) by two analog outputs of an AWG via an IQ mixer. A rapid microwave switch makes sure that the sample is protected from the noise at the amplifier except when the pulses are on. The input line is strongly attenuated at low-temperatures in order to thermalize the microwave field to millikelvin temperature. The pulses are routed to the sample via a circulator, and the reflected signal is routed to the output line. It then undergoes amplification at several stages, starting from a JPA at 12 mK, followed by a HEMT at 4 K and then at room-temperature. The signal is finally demodulated using an IQ mixer, and its two quadratures digitized. (For interpretation of the references to colour in this figure legend, the reader is referred to the web version of this article.)

spectroscopy [5,13], increased ENDOR sensitivity [14], and optimal control [15–18]. They have also been applied for fast superconducting qubit state manipulation [19] and readout [20]. Recently, a new generation of ESR spectrometers has been demonstrated, relying on superconducting micro-resonators and amplifiers cooled at millikelvin temperatures to reach sensitivity below 100 spin/ $\sqrt{\text{Hz}}$ [21–23]. Pulse transients are particularly relevant in these experiments since the superconducting resonators can have high quality factors, in the 10^4 – 10^5 range. Here we demonstrate cavity transient compensation using shaped-pulses in such a quantum-limited ESR spectrometer. We show that shaped pulses enable cavity ringdown suppression, wide-band spin manipulation, as well as signal-to-noise-ratio enhancement.

2. Theory

We consider here a cavity with a single input/output port. We describe the intra-cavity field in its rotating frame at frequency ω_0 by the two quadratures $X(t), Y(t)$ expressed in dimensionless

units, using standard input-output theory [24]. The coupling rate to the input port is denoted as κ_c , whereas the total damping rate $\kappa = \kappa_c + \kappa_i$ also includes the internal cavity loss rate κ_i .

The cavity is coupled to an ensemble of N spins $1/2$ with spin operators $S_{x,y,z}^{(j)}$. The equations that govern the evolution of spin j are

$$\begin{cases} \dot{S}_x^{(j)} = -\Delta_j S_y^{(j)} + g_j Y S_z^{(j)} \\ \dot{S}_y^{(j)} = \Delta_j S_x^{(j)} - g_j X S_z^{(j)} \\ \dot{S}_z^{(j)} = g_j X S_y^{(j)} - g_j Y S_x^{(j)}, \end{cases} \quad (1)$$

where g_j is the spin-resonator coupling constant [21] (which is proportional to the amplitude of B_1 at the spin location), and $\Delta_j = \omega_j - \omega_0$ is the detuning from the resonator frequency. These are identical to the usual Bloch equations, with the Rabi frequency given by the product of the coupling constant g_j and the corresponding field quadrature amplitude [25]. The cavity field is coupled both to the input drive field quadratures $\beta_{x,y}(t)$ and to the spins via

$$\begin{cases} \dot{X}(t) = \sqrt{\kappa_c} \beta_x(t) - \frac{\kappa}{2} X(t) - \sum_{j=1}^N 2g_j S_y^{(j)} \\ \dot{Y}(t) = \sqrt{\kappa_c} \beta_y(t) - \frac{\kappa}{2} Y(t) + \sum_{j=1}^N 2g_j S_x^{(j)}. \end{cases} \quad (2)$$

Eqs. (1) and (2) enable to compute the intra-cavity field and spin dynamics for a given drive field $\beta_{x,y}(t)$, provided the distributions of spin Larmor frequency $\rho_\Delta(\Delta)$ and coupling constant $\rho_g(g)$ (caused by the spatial inhomogeneity of the B_1 field) are known. Here we are interested in finding the drive fields $\beta_{x,y}(t)$ to achieve a given intracavity field profile specified by the quadratures $X_p(t), Y_p(t)$. This problem is drastically simplified if the field generated by the spins (third term on the right of Eqs. (2)) is negligible compared to the intracavity field produced by the drive field. That is the case when the so-called cooperativity parameter $C = \sum_j g_j^2 / (\kappa \bar{\Delta})$ verifies $C \ll 1$ [25] ($\bar{\Delta}$ being the characteristic width of the $\rho_\Delta(\Delta)$ distribution), which is the usual situation in both NMR and ESR. In the following we will assume to be in this situation. A targeted dynamics $[X_p(t), Y_p(t)]$ is then obtained with the drive fields

$$\begin{cases} \beta_x(t) = [\dot{X}_p(t) + \frac{\kappa}{2} X_p(t)] / \sqrt{\kappa_c} \\ \beta_y(t) = [\dot{Y}_p(t) + \frac{\kappa}{2} Y_p(t)] / \sqrt{\kappa_c}, \end{cases} \quad (3)$$

which is identical to the formula derived in [2]. Our target pulse shape in this work is the so-called “bump pulse”, defined as

$$X_p(t) = X_0 e^{-1/|1 - (t/t_p)^2|}, Y_p(t) = 0, \quad (4)$$

for $|t| < t_p/2$, and $X_p(t) = Y_p(t) = 0$ for $|t| \geq t_p/2$. X_0 denotes the maximum amplitude and t_p the pulse length. This pulse shape goes smoothly to zero at $\pm t_p/2$ and does not need to be truncated, contrary to Gaussian pulses for instance [25]. From Eq. (3), the time-dependent drive pulse needed to obtain a bump-shaped intracavity field is readily obtained.

In the experiment, we detect the field leaking out of the cavity. The latter contains both the reflected drive pulses, as well as the spin free-induction-decay and echo signals. The output field quadratures are given by the input-output relation

$$\begin{cases} X_{out}(t) = \sqrt{\kappa_c} X(t) - \beta_x(t) \\ Y_{out}(t) = \sqrt{\kappa_c} Y(t) - \beta_y(t). \end{cases} \quad (5)$$

In the following, we resort to numerical simulations to compare our model to the experimental results. For that, we first compute the distributions $\rho_g(g)$ and $\rho_\Delta(\Delta)$. We then discretize these distri-

butions into $N_g \times N_\Delta$ bins of spins with identical coupling and frequency. We integrate $N_g \times N_\Delta$ times Eq. (1) and finally compute the cavity and output fields using Eqs. (2) and (5).

All that precedes is the standard treatment of inductively-detected magnetic resonance, be it nuclear or electronic. One specific aspect of our experiments is that due to the small mode volume, high quality factor of the superconducting micro-resonator, and to the low temperature of the experiments, spins relax towards thermal equilibrium dominantly by spontaneous emission of a microwave photon into the cavity [26] – the so-called Purcell effect. The Purcell relaxation rate for spin j is given by

$$\Gamma_{1j} = \kappa \frac{g_j^2}{\Delta_j^2 + \kappa^2/4}. \quad (6)$$

In our experiments, Purcell relaxation plays no role during a spin-echo sequence because it occurs on a much longer timescale, which is why it was not included in Eqs. (1). It however plays a role in the steady-state polarization profile of the spin-ensemble, because of the dependence of the relaxation rate on the detuning and coupling constant. We take this phenomenon into account by initializing the density matrix of spin j at $t = 0$ as $\rho_j = [-1 + e^{-\Gamma_{1j}t}]S_z$, t_r being the repetition time of the experimental sequence.

3. Materials and methods

The spectrometer is built around a superconducting micro-resonator that was described in [23]. It consists of an Aluminum thin-film patterned as a lumped-element LC circuit with a 100 μm -long, 500 nm-wide inductance, on top of a silicon substrate [see Fig. 1(b)]. This inductance defines the active area of the resonator around which B_1 is sizeable and spins are therefore detected; the corresponding mode volume is ~ 0.2 pL. Finite-element modelling yields the spatial distribution of the B_1 field generated around the inductance, which in turn allows us to compute the coupling constant density function $\rho_g(g)$ needed in the simulations. As explained in [23], the average coupling constant over the detection volume is found to be $g/2\pi \sim 450$ Hz.

The resonator chip is mounted in a sample holder which is cooled down at 12 mK in a dilution refrigerator. The 50 Ω coaxial line used for delivering the control pulses and collecting the signal is connected to the sample holder with a SMA bulkhead to which an antenna is soldered [21]. By tuning the antenna length, one can adjust the capacitive coupling of the resonator to the line and thus its quality factor ($Q \sim 4 \times 10^4$ in this work). Spectroscopic measurements allow us to extract the resonance frequency $\omega_0/2\pi = 7.274$ GHz, the coupling rate $\kappa_c = 7.1 \cdot 10^5 \text{ s}^{-1}$, the internal energy loss rate $\kappa_i = 2.8 \cdot 10^5 \text{ s}^{-1}$ (measured at the single photon limit), and the total energy loss rate $\kappa = 10^6 \text{ s}^{-1}$. The corresponding field decay time is $2/\kappa = 2 \mu\text{s}$.

An overview of both the low-temperature part of the setup and the room-temperature electronics is schematically shown in Fig. 1 (c). The input line is heavily attenuated at low temperatures to thermalize the microwave field close to the cryostat base temperature. A circulator routes drive pulses from the input waveguide towards the sample, and the reflected signal (together with the spin signal) towards the output waveguide. It is amplified first at 12 mK by a quantum-limited Josephson Parametric Amplifier (JPA) [27], then at 4 K by a High-Electron-Mobility-Transistor (HEMT), and at room-temperature for the final amplification stage. After demodulation by mixing with the local oscillator, the down-converted signal is sampled by a digitizer yielding the field quadratures $I(t), Q(t)$ (in the following only the signal-carrying quadrature is shown). Note that due to the unusually small resonator mode volume, low microwave powers (of order picoWatt)

are needed to drive the spins; as a result, we can measure with the exact same setup both the drive pulses after their reflection at the resonator input and the spin signal, which is useful for the shaped pulses characterization. More details on the resonator, JPA, and spectrometer design, can be found in [21,23]. In [23] the spin detection sensitivity was estimated to be 65 spin/ $\sqrt{\text{Hz}}$ for the same setup but with a quality factor of $8 \cdot 10^4$. Assuming that the sensitivity scales like κ (since the echo amplitude scales like $1/\sqrt{\kappa}$ and the repetition time like κ), we estimate it to be in the present case ~ 150 spin/ $\sqrt{\text{Hz}}$.

One issue with superconducting micro-resonators is their low power handling capability. Indeed, in a superconducting strip such as used for the inductance, non-linear effects appear when the current density approaches the critical current density of the film. For Aluminum at low temperatures it is of order 10^{11} A/m² [28], which implies that in our geometry non-linear effects are expected for ~ 1 mA ac current in the wire. Because of the large spin-resonator constant however, spins can be driven efficiently well below that threshold as will be shown in the following.

In order to generate microwave drive pulses with arbitrarily-controlled amplitude and phase, we modulate the continuous signal delivered by a microwave synthesizer (the local oscillator LO) using two analog outputs of an AWG (model Tektronix 5014), using an IQ mixer. The AWG sampling rate is 1 Gs/s, and its analog bandwidth is 300 MHz. After calibration of the IQ mixer, LO leakage was ~ 60 dB. At the mixer output, the pulse goes through a voltage-controlled attenuator and is then amplified to obtain sufficient driving strength. Right before the low-temperature part of the setup, a fast microwave switch controlled by a digital output of the AWG with 80 dB dynamics transmits microwave signals into the cryostat only during the application of the drive pulses. This protects the spins from the amplifier output noise, which would otherwise reduce their equilibrium polarization [29]. Phase cycling is performed using the IQ modulation by the AWG.

To test the spectrometer operation with shaped pulses, we use the electron-spin resonance of bismuth donors in silicon as a model system. Bismuth atoms were implanted into the silicon sample on which the resonator is patterned, at a typical depth of 100 nm. At low temperatures, bismuth atoms can bind an electron; details on the spin Hamiltonian of such bismuth donors can be found in [30,31]. A field $B_0 = 3.74$ mT is applied in order to tune the lowest-frequency transition of the bismuth donors in resonance with ω_0 . As explained in [21,32,23] the spin resonance of the donors in our experiment is broadened by strain in the substrate caused by thermal contraction of the thin-film resonator upon cooling, which affects inhomogeneously the hyperfine coupling constant between the bismuth nuclear and electron spins. The resulting spin linewidth was measured to be of order ~ 20 – 30 MHz [23], considerably larger than the 200 kHz resonator linewidth. This situation is frequently encountered in ESR spectroscopy. In the simulations we will therefore model the spin density $\rho_\Delta(\Delta)$ as being a constant.

4. Experimental results

4.1. Shaped pulse characterization

In NMR and ESR experiments using shaped pulses, the intracavity field is often characterized by inserting a pickup coil in the resonator [3,9,17], or by using the Rabi nutation of the spins [5]. Here we directly measure the reflected drive pulse, and use it to extract the intra-cavity field. This is facilitated by the low microwave power (picoWatts at the sample level) of the drive pulses used in our experiments, which is itself a consequence of the large spin-resonator coupling.

As can be seen from Eq. (5), the intra-cavity field can be obtained by subtracting the reflected signal from the incident drive pulse, both measured with the very same setup. To do so, we measure the reflected pulse at ω_0 , whereas the incident pulse is measured by applying it 10 MHz off-resonance from ω_0 , so that it is fully reflected at its input without deformation. Because of the small frequency difference, the transfer function of the whole setup can be considered identical in both cases, so that the signals can be simply subtracted, yielding the intra-cavity field $X(t), Y(t)$.

Examples are shown in Fig. 2 (only the quadrature carrying the signal is displayed). For a 1 μs -long square-shaped pulse, the intra-cavity field shows a linear rise during the pulse, followed by an exponential decay with a time constant of $\sim 2/\kappa$ as expected. We then generate a “bump” pulse with $t_p = 1 \mu\text{s}$ (Eq. (4)), using Eqs. (3) to compute the AWG drives [2]. The measured intra-cavity field of the bump pulse is in excellent agreement with the expected pulse shape as given by Eq. (4), with the maximum amplitude as the only fitting parameter. Transients are efficiently suppressed, by at least an order of magnitude; and the intra-cavity field rise- and decay time is $\sim 250 \text{ ns}$, an order of magnitude shorter than the cavity field decay time $2/\kappa$. This successful transient suppression also confirms that the resonator remains linear upon application of the drive pulses (square as well as bump).

4.2. Echoes with shaped pulses

We proceed with the measurement of spin-echoes, using a $\pi/2\chi - \tau - \pi\gamma - \tau$ Hahn-echo sequence with X/-X phase-cycling on the first pulse. To optimize the pulse amplitude, Rabi nutation data was taken by measuring the integrated echo amplitude A_e as a function of the refocusing pulse amplitude for a square pulse shape (see Fig. 3). Damping of the oscillations is caused by the spread in Rabi frequency $\rho_g(g)$ due to B_1 spatial inhomogeneity, and is qualitatively reproduced by the simulations. Fig. 3 also shows the reflected signal quadrature of a full echo trace, including the echo, both for 1 μs -long square-shaped and bump-shaped pulses. The reflected control pulses again demonstrate transient

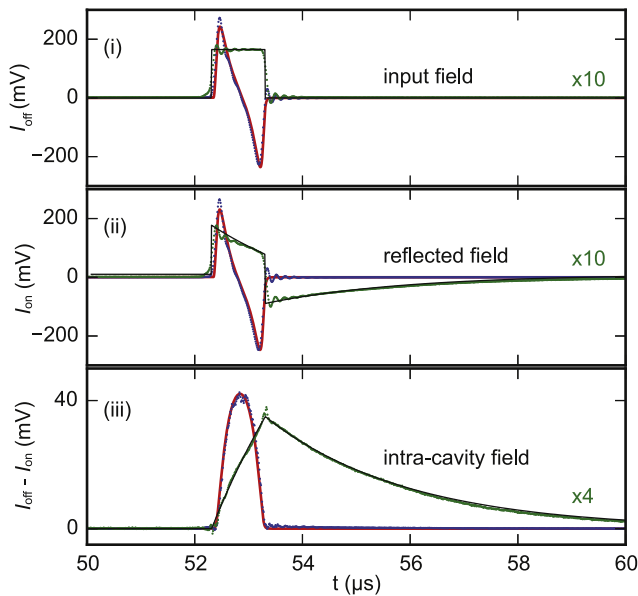


Fig. 2. Reflected quadrature signal of a square (green dots) and bump-shaped (blue dots) pulses, measured 10 MHz off-resonance (i) and on-resonance with ω_0 (ii). Subtraction yields the intra-cavity field (iii). Solid lines are from the theory. The small oscillations probably originate from parasitic resonances in the microwave setup. (For interpretation of the references to colour in this figure legend, the reader is referred to the web version of this article.)

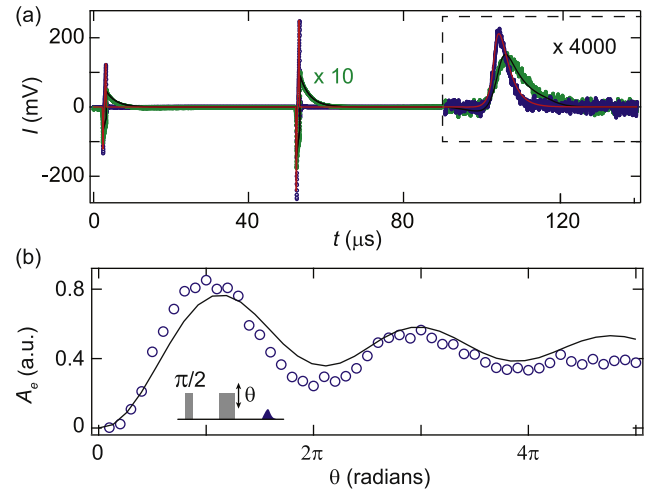


Fig. 3. (a) Hahn-echo sequence with square and bump-shaped pulses. First, a $\pi/2\chi - \tau - \pi\gamma - \tau$ spin-echo was measured (inset). The corresponding control pulses were sampled immediately afterwards, with only a change in amplifier gain at the detection to compensate for the larger signal amplitude. For convenience, the two control pulses were this time generated on the same quadrature, which is shown here in the main panel. Open circles are data (green for square, blue for bump), and solid lines are results from the simulation (black for square, red for bump). (b) Rabi oscillations (blue dots) and simulation (black line) for a square-shaped-pulse Hahn echo sequence with varying refocusing pulse amplitude. (For interpretation of the references to colour in this figure legend, the reader is referred to the web version of this article.)

suppression in the bump-pulse case. The bump-pulse echo is both shorter and higher-amplitude than the square-pulse. These features are well captured by simulations.

We study the shaped pulse echo in more details in Fig. 4. In order to measure the contribution from spins outside of the cavity bandwidth, a low repetition rate is necessary, since those spins relax more slowly than spins at resonance because of the Purcell effect (see Eq. (6)). Fig. 4 shows a time trace of a Hahn echo, measured using bump pulses with $t_p = 1 \mu\text{s}$, and a repetition time

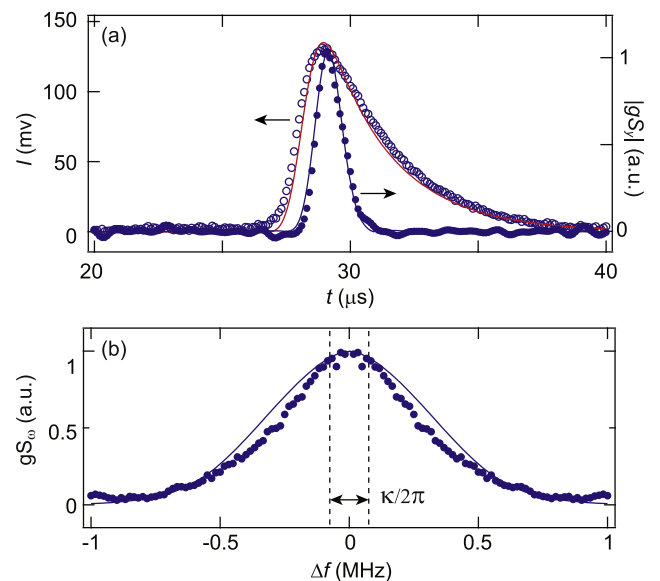


Fig. 4. (a) Quadrature signal of the emitted echo (open circles) and its effective spin component gS_y obtained by de-convolution of the cavity response (filled circles). The measurement is acquired with a repetition time of $t_r = 1 \text{ s}$. (b) Fast Fourier transform of gS_y showing the spectral bandwidth of the echo, much larger than the cavity bandwidth $\kappa/2\pi$. Solid lines are numerical simulations.

$t_r = 1$ s. The echo shows a pronounced asymmetric shape, with a sharp rise in less than a microsecond, and a slower decay. The fact that the echo signal rises faster than $2/\kappa$ demonstrates that the echo originates from the rephasing of spins lying in a broader frequency range than the cavity bandwidth. After the echo reaches its peak amplitude, it decays in $\sim 2/\kappa$. Indeed, despite the use of shaped pulses to drive the spins over arbitrarily wide bandwidth, their emission remains unavoidably filtered by the cavity [5]. To visualize more quantitatively the dynamics of the spin-ensemble magnetization, we have numerically deconvoluted the cavity response (see Fig. 4a inset), resulting in a Gaussian-shaped time dependence with a FWHM width of $1.3 \mu\text{s}$. The Fourier transform of the magnetization is also shown in Fig. 4, and shows a linewidth 4 times greater than κ . Numerical simulations were performed using the computed distributions ρ_g and ρ_Δ , based on the equations of Section II, and taking into account the Purcell relaxation. The echo shape and duration are quantitatively reproduced, as well as the spin magnetization dynamics.

One motivation for short control pulse duration is their higher robustness to spin detuning. Indeed, the nutation frequency of spin j is given by $\sqrt{\omega_1^2 + \Delta_j^2}$, with $\omega_1 = g_j \sqrt{X^2 + Y^2}$. Due to the transient decay, square-shaped pulses have an effective minimum duration of order of $2/\kappa$, implying that the maximum value of ω_1 for a π pulse is $\sim \kappa$. Spins on the edges of the resonator bandwidth (those with $\Delta_i \sim \kappa/2$) therefore unavoidably undergo a Rabi nutation with an angle and axis that are significantly different from those at resonance with a square-shaped pulse. Bump-shaped refocusing pulses on the other hand have a shorter duration, leading to higher ω_1 for a π -pulse and thus to better performance for spins with $\Delta_i \sim \kappa/2$. To test this prediction, we compare the signal-to-noise ratio of an echo obtained with the same square-shaped $\pi/2$ -pulse, but with either a bump- or square-shaped refocusing π pulse. The signal and noise are given by $A_e = \int I(t)u(t) dt$ and $\sigma = \sqrt{\int \delta I^2(t)u^2(t) dt}$, respectively, where $u(t)$ represents the mode shape of the echo normalized such that $\int [u(t)]^2 dt = 1$ [21]. This mode shape is obtained by fitting a skewed Gaussian function to the echo signal

$$u(t) = \frac{1}{\mathcal{N}} \exp \left[-\frac{(t-t_0)^2}{2\sigma^2} \right] \text{erfc} \left[\alpha \frac{t-t_0}{\sigma\sqrt{2}} \right], \quad (7)$$

where \mathcal{N} is the normalization, σ the scale and α the shape factor. We find a SNR improvement of 16% in the bump refocusing pulse case compared to square-pulse refocusing, which confirms the better performance of bump-shaped refocusing pulses.

Suppression of cavity ringdown enables to minimize the delay between control pulses, which is particularly useful for dynamical decoupling pulse sequences where refocusing pulses are applied shortly one after the other. As a proof-of-principle, we run a Carr-Purcell-Meiboom-Gill pulse sequence using bump pulses. Even with a delay of $10 \mu\text{s}$, the echoes are still clearly separated as seen in Fig. 5; whereas with square pulses the minimal separation was found to be closer to $50 \mu\text{s}$. Because of the short delay and long coherence time of donors in silicon (particularly with silicon isotopically enriched in nuclear-spin-free ^{28}Si as in our experiment), ~ 1000 echoes can be measured in this way (see Fig. 5). Such a long echo train may be used in particular for further increasing the single-shot signal-to-noise [33,23]. The shorter inter-pulse delay within the CPMG sequence reduces the sensitivity to higher frequency noise contributions, which enables more echoes to be generated and thus further SNR enhancement. Here, assuming a white-noise background, the CPMG averaging would translate into a SNR improvement as high as a factor 20. Recent experiments however have shown that this figure is over-

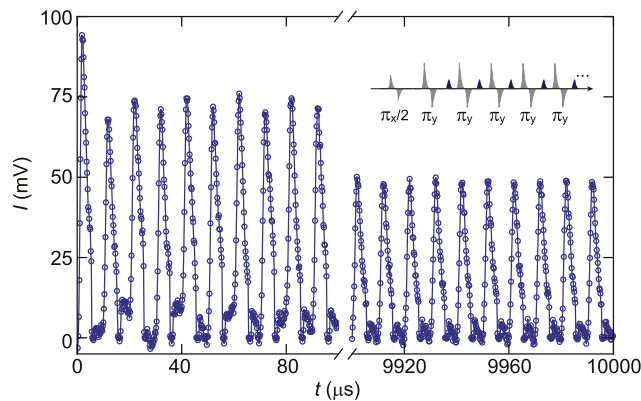


Fig. 5. Averaged CPMG sequence with minimal pulse separation using bump pulses. The π pulses are not visible as they are being canceled by phase cycling.

estimated in the presence of low-frequency or correlated noise, which may occur in experiments with SC resonators due to resonator phase noise [34,23] or long-term spin fluctuations.

5. Conclusions

We have demonstrated cavity ringdown suppression and wide-band spin excitation using shaped control pulses in a high-sensitivity, quantum-limited ESR spectrometer at millikelvin temperatures. So far only bump pulses were used, which were shown to robustly suppress cavity transients and increase the SNR of Hahn-echoes by 16%. Implementing optimal control techniques for special-purpose pulse sequences [17,11,18,35] would be a natural next step to further improve the level of spin control achieved. Also, the ringdown suppression demonstrated here would enable to measure spins with short coherence times, bringing quantum-limited ESR spectroscopy one step closer to real-world applications.

Acknowledgements

We acknowledge technical support from P. Sénat, D. Duet, J.-C. Tack, P. Pari, P. Forget, as well as useful discussions within the Quantronics group. We acknowledge support of the European Research Council under the European Community's Seventh Framework Programme (FP7/2007–2013) through grant agreement No. 615767 (CIRQUSS), of the Agence Nationale de la Recherche through the project QIPSE and the Chaire Industrielle NASNIQ. This project has received funding from the European Unions Horizon 2020 research and innovation program under Marie Skłodowska Curie Grant Agreement No. 765267 (QuSCO) and from the Deutsche Forschungsgemeinschaft (DFG, German Research Foundation) under Germanys Excellence Strategy EXC-2111 390814868.

References

- [1] A. Schweiger, G. Jeschke, *Principles of Pulse Electron Paramagnetic Resonance*, Oxford University Press, 2001.
- [2] K. Takeda, Y. Tabuchi, M. Negoro, M. Kitagawa, Active compensation of rf-pulse transients, *J. Magn. Reson.* 197 (2) (2009) 242–244, <https://doi.org/10.1016/j.jmr.2008.12.012>.
- [3] Y. Tabuchi, M. Negoro, K. Takeda, M. Kitagawa, Total compensation of pulse transients inside a resonator, *J. Magn. Reson.* 204 (2) (2010) 327–332, <https://doi.org/10.1016/j.jmr.2010.03.014>, <<http://www.sciencedirect.com/science/article/pii/S1090780710000844>>.
- [4] T. Kaufmann, T.J. Keller, J.M. Franck, R.P. Barnes, S.J. Glaser, J.M. Martinis, S. Han, DAC-board based X-band {EPR} spectrometer with arbitrary waveform control, *J. Magn. Reson.* 235 (2013) 95–108, <https://doi.org/10.1016/j.jmr.2013.07.015>.

- [5] A. Doll, G. Jeschke, Fourier-transform electron spin resonance with bandwidth-compensated chirp pulses, *J. Magn. Reson.* 246 (Supplement C) (2014) 18–26, <https://doi.org/10.1016/j.jmr.2014.06.016>.
- [6] H. Geen, R. Freeman, Band-selective radiofrequency pulses, *J. Magn. Reson.* (1969) 93 (1) (1991) 93–141, [https://doi.org/10.1016/0022-2364\(19\)90034-Q](https://doi.org/10.1016/0022-2364(19)90034-Q) (<<http://www.sciencedirect.com/science/article/pii/S002223649190034Q>>).
- [7] M. Mehring, J.S. Waugh, Phase transients in pulsed NMR spectrometers, *Rev. Sci. Instrum.* 43 (4) (1972) 649–653, <https://doi.org/10.1063/1.1685714>, <<https://aip.scitation.org/doi/abs/10.1063/1.1685714>>.
- [8] W. Rhim, D.D. Elleman, L.B. Schreiber, R.W. Vaughan, Analysis of multiple pulse NMR in solids. II, *J. Chem. Phys.* 60 (11) (1974) 4595–4604, <https://doi.org/10.1063/1.1680944>, <<https://aip.scitation.org/doi/abs/10.1063/1.1680944>>.
- [9] J.J. Wittmann, K. Takeda, B.H. Meier, M. Ernst, Compensating pulse imperfections in solid-state NMR spectroscopy: a key to better reproducibility and performance, *Angew. Chem. Int. Ed.* 54 (43) (2015) 12592–12596, <https://doi.org/10.1002/anie.201504782>.
- [10] P.E. Spindler, P. Schöps, W. Kallies, S.J. Glaser, T.F. Prisner, Perspectives of shaped pulses for EPR spectroscopy, *J. Magn. Reson.* 280 (2017) 30–45, <https://doi.org/10.1016/j.jmr.2017.02.023>, <<http://www.sciencedirect.com/science/article/pii/S1090780717300617>>.
- [11] T.W. Borneman, D.G. Cory, Bandwidth-limited control and ringdown suppression in high-Q resonators, *J. Magn. Reson.* 225 (Supplement C) (2012) 120–129, <https://doi.org/10.1016/j.jmr.2012.10.011>.
- [12] J.M. Franck, R.P. Barnes, T.J. Keller, T. Kaufmann, S. Han, Active cancellation – a means to zero dead-time pulse EPR, *J. Magn. Reson.* 261 (2015) 199–204, <https://doi.org/10.1016/j.jmr.2015.07.005>, <<http://www.sciencedirect.com/science/article/pii/S1090780715001573>>.
- [13] A. Doll, G. Jeschke, Wideband frequency-swept excitation in pulsed EPR spectroscopy, *J. Magn. Reson.* 280 (Supplement C) (2017) 46–62, <https://doi.org/10.1016/j.jmr.2017.01.004>.
- [14] C.E. Tait, S. Stoll, ENDOR with band-selective shaped inversion pulses, *J. Magn. Reson.* 277 (2017) 36–44, <https://doi.org/10.1016/j.jmr.2017.02.007>, <<http://www.sciencedirect.com/science/article/pii/S1090780717300393>>.
- [15] J.S. Hodges, J.C. Yang, C. Ramanathan, D.G. Cory, Universal control of nuclear spins via anisotropic hyperfine interactions, *Phys. Rev. A* 78 (1) (2008) 010303, <https://doi.org/10.1103/PhysRevA.78.010303>, <<https://link.aps.org/doi/10.1103/PhysRevA.78.010303>>.
- [16] Y. Zhang, C.A. Ryan, R. Laflamme, J. Baugh, Coherent control of two nuclear spins using the anisotropic hyperfine interaction, *Phys. Rev. Lett.* 107 (17) (2011) 170503, <https://doi.org/10.1103/PhysRevLett.107.170503>, <<https://link.aps.org/doi/10.1103/PhysRevLett.107.170503>>.
- [17] P.E. Spindler, Y. Zhang, B. Endeward, N. Gershernzon, T.E. Skinner, S.J. Glaser, et al., Shaped optimal control pulses for increased excitation bandwidth in EPR, *J. Magn. Reson.* 218 (Supplement C) (2012) 49–58, <https://doi.org/10.1016/j.jmr.2012.02.013>.
- [18] S.J. Glaser, U. Boscain, T. Calarco, C.P. Koch, W. Köckenberger, R. Kosloff, I. Kuprov, B. Luy, S. Schirmer, T. Schulte-Herbrüggen, D. Sugny, F.K. Wilhelm, et al., Training Schrödinger's cat: quantum optimal control, *Euro. Phys. J. D* 69 (12) (2015) 279, <https://doi.org/10.1140/epjd/e2015-60464-1>.
- [19] F. Motzoi, J.M. Gambetta, P. Rebentrost, F.K. Wilhelm, Simple pulses for elimination of leakage in weakly nonlinear qubits, *Phys. Rev. Lett.* 103 (11) (2009) 110501, <https://doi.org/10.1103/PhysRevLett.103.110501>, <<https://link.aps.org/doi/10.1103/PhysRevLett.103.110501>>.
- [20] E. Jeffrey, D. Sank, J. Mutus, T. White, J. Kelly, R. Barends, Y. Chen, Z. Chen, B. Chiaro, A. Dunswoth, A. Megrant, P. O'Malley, C. Neill, P. Roushan, A. Vainsencher, J. Wenner, A. Cleland, J.M. Martinis, et al., Fast accurate state measurement with superconducting qubits, *Phys. Rev. Lett.* 112 (19) (2014) 190504, <https://doi.org/10.1103/PhysRevLett.112.190504>.
- [21] A. Bienfait, J. Pla, Y. Kubo, M. Stern, X. Zhou, C.-C. Lo, C. Weis, T. Schenkel, M. Thewalt, D. Vion, D. Esteve, B. Julsgaard, K. Moelmer, J. Morton, P. Bertet, et al., Reaching the quantum limit of sensitivity in electron spin resonance, *Nat. Nanotechnol.* 11 (2015) 253–257, <https://doi.org/10.1038/nnano.2015.282>.
- [22] C. Eichler, A.J. Sigillito, S.A. Lyon, J.R. Petta, Electron spin resonance at the level of 10^4 spins using low impedance superconducting resonators, *Phys. Rev. Lett.* 118 (3) (2017) 037701, <https://doi.org/10.1103/PhysRevLett.118.037701>.
- [23] S. Probst, A. Bienfait, P. Campagne-Ibarcq, J.J. Pla, B. Albanese, J.F.D.S. Barbosa, T. Schenkel, D. Vion, D. Esteve, K.M. Imer, J.J.L. Morton, R. Heeres, P. Bertet, et al., Inductive-detection electron-spin resonance spectroscopy with 65 spins/ $\sqrt{\text{Hz}}$ sensitivity, *Appl. Phys. Lett.* 111 (20) (2017) 202604, <https://doi.org/10.1063/1.5002540>.
- [24] C.W. Gardiner, M.J. Collett, Input and output in damped quantum systems: quantum stochastic differential equations and the master equation, *Phys. Rev. A* 31 (6) (1985) 3761, <https://doi.org/10.1103/PhysRevA.31.3761>, <<http://link.aps.org/doi/10.1103/PhysRevA.31.3761>>.
- [25] Q. Ansel, S. Probst, P. Bertet, S.J. Glaser, D. Sugny, Optimal control of an inhomogeneous spin ensemble coupled to a cavity, *Phys. Rev. A* 98 (2) (2018) 023425, <https://doi.org/10.1103/PhysRevA.98.023425>, <<https://link.aps.org/doi/10.1103/PhysRevA.98.023425>>.
- [26] A. Bienfait, J. Pla, Y. Kubo, X. Zhou, M. Stern, C.-C. Lo, C. Weis, T. Schenkel, D. Vion, D. Esteve, J. Morton, P. Bertet, et al., Controlling spin relaxation with a cavity, *Nature* 531 (2016) 74–77, <https://doi.org/10.1038/nature16944>.
- [27] X. Zhou, V. Schmitt, P. Bertet, D. Vion, W. Wustmann, V. Shumeiko, et al., High-gain weakly nonlinear flux-modulated Josephson parametric amplifier using a SQUID array, *Phys. Rev. B* 89 (21) (2014) 214517, <https://doi.org/10.1103/PhysRevB.89.214517>.
- [28] J. Romijn, T.M. Klapwijk, M.J. Renne, J.E. Mooij, Critical pair-breaking current in superconducting aluminum strips far below T_c , *Phys. Rev. B* 26 (7) (1982) 3648–3655, <https://doi.org/10.1103/PhysRevB.26.3648>, <<https://link.aps.org/doi/10.1103/PhysRevB.26.3648>>.
- [29] A. Bienfait, P. Campagne-Ibarcq, A. Kiilerich, X. Zhou, S. Probst, J. Pla, T. Schenkel, D. Vion, D. Esteve, J. Morton, K. Moelmer, P. Bertet, et al., Magnetic resonance with squeezed microwaves, *Phys. Rev. X* 7 (4) (2017) 041011, <https://doi.org/10.1103/PhysRevX.7.041011>, <<https://link.aps.org/doi/10.1103/PhysRevX.7.041011>>.
- [30] R.E. George, W. Witzel, H. Riemann, N.V. Abrosimov, N. Nötzel, M.L.W. Thewalt, et al., Electron spin coherence and electron nuclear double resonance of bi donors in natural si, *Phys. Rev. Lett.* 105 (6) (2010) 067601, <https://doi.org/10.1103/PhysRevLett.105.067601>, <<https://link.aps.org/doi/10.1103/PhysRevLett.105.067601>>.
- [31] G. Wolfowicz, A.M. Tyryshkin, R.E. George, H. Riemann, N.V. Abrosimov, P. Becker, H.-J. Pohl, M.L.W. Thewalt, S.a. Lyon, J.J.L. Morton, et al., Atomic clock transitions in silicon-based spin qubits, *Nat. Nanotechnol.* 8 (June) (2013) 561–564, <https://doi.org/10.1038/nnano.2013.117>.
- [32] J. Pla, A. Bienfait, G. Pica, J. Mansir, F. Mohiyaddin, Z. Zeng, Y. Niquet, A. Morello, T. Schenkel, J. Morton, P. Bertet, et al., Strain-induced spin-resonance shifts in silicon devices, *Phys. Rev. Appl.* 9 (4) (2018) 044014, <https://doi.org/10.1103/PhysRevApplied.9.044014>, <<https://link.aps.org/doi/10.1103/PhysRevApplied.9.044014>>.
- [33] F. Mentink-Vigier, A. Collauto, A. Feintuch, I. Kaminker, V. Tarle, D. Goldfarb, Increasing sensitivity of pulse (EPR) experiments using echo train detection schemes, *J. Magn. Reson.* 236 (2013) 117–125, <https://doi.org/10.1016/j.jmr.2013.08.012>.
- [34] J. Gao, J. Zmuidzinas, B.A. Mazin, H.G. LeDuc, P.K. Day, Noise properties of superconducting coplanar waveguide microwave resonators, *Appl. Phys. Lett.* 90 (10) (2007) 102507, <https://doi.org/10.1063/1.2711770>.
- [35] W. Kallies, S.J. Glaser, Cooperative broadband spin echoes through optimal control, *J. Magn. Reson.* 286 (2018) 115–137, <https://doi.org/10.1016/j.jmr.2017.10.011>, <<http://www.sciencedirect.com/science/article/pii/S1090780717302641>>.